Oscillatory electro-oxidation of thiosulfate on gold

Wenyan Bi,[1,2] Yuxiu He,[1] Murilo F. Cabral,[3] Hamilton Varela,[3,4,*] Jiaping Yang,[1] Rongli Jiang,[1] Qingyu Gao[1,*]

[1]College of Chemical Engineering, China University of Mining and Technology, Xuzhou 221008, China

[2]School of Physics and Chemistry, Henan Polytechnic University, Jiaozuo 454000, China

[3]Institute of Chemistry of São Carlos, University of São Paulo, P.O. Box 780, 13560-970, São Carlos, SP, Brazil

[4]Fritz Haber Institute of the Max Planck Society, Department of Physical Chemistry, Faradayweg 4-6, D-14195 Berlin, Germany

Abstract

We report experimental results on the oscillatory electro-oxidation of thiosulfate on polycrystalline gold electrode in buffered media of pH 6.0. Importantly, we observed oscillations in the current density (potential) when the system was studied under linear sweep of potential (current density). The system displays supercritical Hopf, period-doubling, homoclinic and bursting bifurcations at different applied currents and potentials. After presenting the dynamics under both potentiostatic and galvanostatic regimes, we characterized the system in terms of its electrical (ohmic drop compensation and electrochemical impedance spectroscopy) and chemical (Capillary Electrophoresis analysis) aspects. Ohmic resistance compensation and electrochemical impedance spectroscopy confirmed the hidden N-shaped negative differential resistance oscillatory character. Capillary electrophoresis analysis revealed the predominance of different oxidation products as a function of the applied potential. Finally, we suggest a tentative mechanism underlying the kinetic instabilities.

Keywords: thiosulfate, gold, electro-oxidation, bifurcation, mixed mode oscillations.

Corresponding authors: gaoqy@cumt.edu.cn, varela@iqsc.usp.br

HV: ISE Member

1. Introduction

Thiosulfate is a very important chemical substance in fields such as chemical synthesis, biological chemistry, wastewater treatment, mineral separation, paper manufacturing and photographic industry [1-3]. Thiosulfate can be oxidized chemically or electrochemically to sulfate and, as a number of intermediate oxidation states are possible, rather complex reaction mechanisms are commonly observed. The oxidation of thiosulfate is generally associated with rich nonlinear behavior in chemical and electrochemical systems [4-11]. Many homogeneous chemical reactions exhibiting autocatalysis and sustained oscillations have been reported, including the chlorite-thiosulfate [4-5], bromate-thiosulfate [6], periodate-thiosulfate [7] and peroxide-thiosulfate [8-10] systems. The electrocatalytic oxidation of thiosulfate on platinum surfaces can also result in interesting dynamics, including the emergence of period-doubled, mixed-mode, and quasiperiodic oscillations, and chaos [11].

Most studies on the nonlinear phenomena observed during the electro-oxidation reactions at the solid/liquid interfaces are conducted on platinum surfaces. This is due to the high electrocatalytic activity of platinum towards many reactions, including the dehydrogenation and oxidation of small organic molecules and the oxidation of molecular hydrogen [12, 13]. Expanding the current knowledge of electrochemical oscillations to reactions on other surfaces is a major step towards the understanding of surface processes underlying complex chemical kinetics at the electrified solid/liquid interface. This is also of importance when considering the possibilities of application and development of other imaging techniques.

Gold is a noble and relatively inert metal, and is a very weak chemisorber, which in the presence of pure electrolytes shows only non-Faradaic processes over a wide potential region, and exhibits a monolayer (or Au_2O_3) oxide formation/removal reaction at quite positive potentials[14-17]. However, many electrocatalytic reactions on gold surfaces were

observed in aqueous media, and were commonly discussed in terms of the active states of gold and explained by the IHOAM (incipient hydrous oxide/adatom mediator) model [17]. The IHOAM model also rationalizes the high catalytic activity of oxide-supported gold microparticles as reported by Haruta and co-workers [18]. The electrocatalytic reduction of periodate [19] and of molecular oxygen and hydrogen peroxide on Au (100) in alkaline media [20] are examples of the rare reports to date on oscillatory kinetics on gold surfaces. There are apparently no reports of instabilities in electro-oxidation reactions, in spite of the considerably high electrochemical activity towards the oxidation of carbon monoxide and small alcohols in alkaline media [21-24].

We report in this paper a comprehensive experimental investigation of the electro-oxidation of sodium thiosulfate on polycrystalline gold, with emphasis on the self-organized potential and current density oscillations. The study was performed in phosphate buffer (pH 6.0) and the system investigated using cyclic voltammetry (CV), chronoamperometry, chronopotentiometry, and electrochemical impedance spectroscopy (EIS). Furthermore, Capillary Electrophoresis (CE) analysis was also employed to infer on the chemical identity of soluble oxidation products.

2. Experimental Section

All electrochemical experiments were performed at 20 ^{o}C by a computer controlled Autolab PGSTAT 302N electrochemical workstation (Metrohm Ltd., Switzerland). The electrochemical set-up use is depicted in Figure 1. A conventional three-electrode electrochemical cell with a volume of 100 mL was used. A gold disk with a diameter of 20.0 mm, embedded in an insulating Teflon cylinder served as the working electrode (WE). The counter electrode (CE) was a gold thin foil 10 cm long, 1 cm wide and 0.02 cm thick, bended into a circular shape. The top edges of the CE and the bottom plane of the WE were arranged

in the same plane, c.f. Figure 1. A reversible hydrogen electrode (RHE), made with a "J" glass tube in which 0.5 mol cm^{-3} H_2SO_4 was used as the electrolyte, was placed between WE and CE was used as the reference electrode (RE). A charge-coupled-device (CCD) camera under the quartz window was adopted to observe the WE surface. Both working electrode and the electrolyte solution were kept stationary in all experiments. Potentials measured (or controlled) in all experiments are referred to the RHE scale. Electrolyte solutions were prepared by dissolving appropriate amounts of analytical grade sodium thiosulfate (Johnson Mattey Company) in ultrapure water (Millipore system, 18.2 MΩ·cm). Buffer solutions of NaH_2PO_4-Na_2HPO_4 were used to maintain the electrolyte pH 6.0. The capillary electrophoresis (CE) analysis was performed on a CE-based analytical system P/ACE MDQ (Beckman) equipped with a diode array detector (DAD). A fused-silica capillary of 57.0 cm (50.0 cm to the detector) × 75 μm i.d. × 375 μm o.d. was used. The sample was injected into the capillary by overpressure. A negative voltage of 30 kV was applied for separation, and 195.0 nm was selected for the spectrophotometric detection.

Before each experiment, the gold disk was firstly polished to a mirror-like shine with diamond suspension (1 μm) on a Buehler polishing microcloth of a polishing machine (MetaServ 250, Buehler, USA), and then was immersed into a mixture of 1% $KMnO_4$ and 30% H_2O_2 at room temperature for 12 hours. After that it was cleaned with ultrapure water. The electrolyte was deareted with purified nitrogen for 20 – 25 min at room temperature. All experiments started with a series of cycling voltammograms between -0.65 and 0.80 V at a scan rate of 0.1 V s^{-1} in 0.500 mol dm^{-3} H_2SO_4, until a constant current density vs potential profile was attained.

3. Results and Discussion

3.1 Potentiodynamic and galvanodynamic profiles

Figure 2 shows the cyclic voltammogram between 0 V and 2.000 V in 1.000 mol dm^{-3} phosphate buffer (pH 6.0) at a scan rate of 0.01 V s^{-1}. It can be seen clearly that the formation of gold oxide occurred around 1.500 V, where two peaks suggest that the different states of gold oxide may be generated [17]. When the electrode potential is higher than about 1.800 V, the current density increases abruptly due to the oxygen evolution as evidenced by gas bubbles on the surface of the WE, as observed by CCD camera. The second reduction peak at around 0.600 V results from β gold oxide (hydrous oxide) yielded by oxidation of metastable metal surface (MMS) gold-atoms [17].

Figure 3 shows both the potential and current linear sweeps curves in 0.400 mol dm^{-3} $Na_2S_2O_3$ with buffer (pH 6.0) on gold electrode. The open circuit potential is 0.200 V under these experimental conditions. In the potentiodynamic sweep experiment from 0 V to 2.000 V shown in Figure 3a, multiple negative differential resistances (NDRs) are discernible. Three main regions can be seen marked with A, B and C. In region A, it is indicated that the NDR is induced by the formation of gold sulfide layer, which blocks surface sites. As a consequence, the current density decreases with increasing potential at around 0.750 V and then it reaches a current plateau around zero, as the electrode is in a passivated state. As the potential increases, the current density gradually increases. Between 1.000 and 1.600 V, two distinct current density oscillations are clearly observed along the positive slope in the current density-potential curve. The first region is in the range of 1.070 – 1.280 V and the other lasts from 1.360 V to 1.400 V. It is speculated that the first oscillatory region is related to the formation of gold oxide and the second oscillatory region possibly corresponds to another gold oxide with higher gold oxidation state in Figure 3.

When the system is driven by a galvanodynamic sweep from 0 to 27.00 mA cm^{-2} (Figure 3b), the electrode potential spontaneously oscillates in two distinct regions (M and N). The first oscillatory region is observed from 7.30 mA cm^{-2} to 8.97 mA cm^{-2}. The second

oscillatory region is confined between 10.15 mA cm^{-2} and 16.25 mA cm^{-2}. The second region is characterized by larger amplitude and lower frequency oscillations, when compared to that in the first one, at lower applied currents density.

3.2 Oscillatory Dynamics

Since two oscillatory regions and complex dynamic characteristics were found along the quasi-stationary linear sweeps, we proceeded in the following a detailed study of the oscillatory dynamics under potentiostatic and galvanostatic control.

Current oscillations. As presented in Figure 3a, there are two oscillatory regions. Figure 4 shows the resulting current density time-series of the electro-oxidation of a solution 0.400 mol dm^{-3} $Na_2S_2O_3$ with buffer (pH 6.0) on gold electrode. In these experiments, the potential was increased from 0 to 2.000 V step by step with 200 s duration at each potential. When the potential was kept lower than about 1.000 V, the current density remained strictly in a stable steady state (SSSI), as shown in Figure 4a. The current density holds at a very low value about 1.40 mA cm^{-2}, which indicates that the gold surface is inactive towards thiosulfate electro-oxidation. This is caused by the formation of gold sulfide layer at the first oxidation region A (Figure 3a), which passivates the surface. As the potential increased to 1.100 V, the system undergoes a supercritical Hopf bifurcation and the current density starts to oscillate with increasingly amplitude, Figure 4b. Further increasing the potential to 1.155 V, period-2 oscillations are induced, Figure 4c. At E = 1.160 V, simple oscillations with high frequency are observed, Figure 4d. Then it changes into 1^1 mixed-mode oscillations at E = 1.185 V, Figure 4e. As the potential is held at 1.230 V, the oscillations turn into more complex ones, namely period-2 of 1^1-type mixed-mode oscillations, i.e. P2(1^1), cf. Figure 3f. When the potential is increased to 1.235 V, the current density oscillates in a 1^2 mixed-mode state,

illustrated in Figure 4g. Then it transforms into P2 (1^2) oscillations at 1.240 V, shown in Figure 4h. 1^3 complex mixed-mode oscillations are found at the potential of 1.320 V, Figure 4i. Further, when the potential is increased from 1.322V, then 1.325V to 1.328 V, the oscillatory mode gradually undergoes an evolution from 1^4, then 1^5 and to 1^6 oscillations in Figure 4j-l. And then the system accesses a more complex oscillating mode of 1^7 oscillations when the potential is increased to 1.330 V (Figure 4m). Finally when the potential is 1.335 V, no oscillations are observed (Figure 4n) and a stable steady state (SSSII) is reached.

From the *j-E* curve in Figure 3a we can also see that the system goes through a supercritical bifurcation, along the potentiodynamic sweep. The first oscillatory region is observed between 1.070 and 1.280 V, and the second one between 1.360 and 1.400 V. Therefore, in the second oscillatory region in Figure 3a, the system undergoes another bifurcation sequence. Under potentiostatic control, the system starts to oscillate in a higher potential region at 1.345 V with the oscillatory mode of 1^1-type. With the potential increasing step by step, oscillations in the current density get more and more complex. As can be seen from Figure 4o-s, the current density firstly oscillates in 1^1 mode, then P2 (1^1) and 1^2, 1^3 to 1^5 modes. When the potential is higher than 1.380 V, the system displays damped oscillations. Finally, it goes to stable steady state (SSSIII) at 1.600 V, seen in Figure 4t.

Figure 5 summarizes the whole sequence of dynamic states described in Figure 4. As already pointed out, there are two potential windows: one from 1.000 V to 1.335 V, the other between 1.335 V and 1.600 V. In the first oscillatory region, the current density transited gradually from stable steady state (SSSI) to simple oscillations (SO), then mixed-mode oscillations of type I (MMO I), and again reached to a new stable steady state (SSSII). In the latter region, the curve goes through the mixed-mode oscillations of type II (MMO II) and damped oscillations (DO), as the potentials is increased. Finally, a stable steady state (SSSIII) is reached.

Potential oscillations. As anticipated in Figure 3b, there are also two oscillatory regions discernible along the galvanodynamic sweep of 0.400 mol dm^{-3} $Na_2S_2O_3$ with buffer (pH 6.0) on gold electrode. The amplitude of the second region is larger than that of the first one. As the applied current density is increased, the first potential platform appears, and then it goes into a oscillatory region. Further current density increase brings a second potential plateau before entering into the second oscillatory region. In this section, we present results obtained under galvanostatic control to further investigate the structure of the potential oscillations in detail.

Figure 6 presents the full set of potential time-series from 0 to 27.00 mA cm^{-2} when the current density was increased step by step with 100 s duration at each step. As the current density is below 0.35 mA cm^{-2}, the potential varying with time gradually increases and then abruptly goes up, and finally stays in a stable steady state (SSSI), as shown in Figure 6a. When the current density is held at 0.35 mA cm^{-2}, the electrode potential oscillates spontaneously in simple mode as shown in Figure 6b. By increasing the applied current density step by step, the potential oscillations evolve in the sequence 1^1, 1^2, 1^3, 1^4, P2 (1^4), 1^5, 1^6 to 1^7, from Figure 5c to j. Other complex structures such as P2 (1^2) and P2 (1^3), $1^2 1^3$, $1^3 1^4$ were also observed, making oscillations in this region abundant and rather intricate.

Further increasing the current density to 2.90 mA cm^{-2}, the system goes to stable steady state (SSSII) again, Figure 6k. This stable steady state lasts in a wide range of applied current density. It would be caused by the formation of gold oxide layer on the electrode. When the current density increases to 3.18 mA cm^{-2}, the potential oscillations transform into simple small oscillations (SO), seen in Figure 6l, before experiencing a bursting bifurcation, Figure 6m. With the current density increases to 4.33 mA cm^{-2}, the potential oscillates in more complex mode, namely mixed-mode oscillations seen in Figure 6n. When current

density is higher than 5 mA cm^{-2}, the system displayed damped oscillations. Then it is noted that the potential stays in stable steady state (SSSIII) again with the current density controlled at 7.90 mA cm^{-2}. When compared to the galvanodynamic sweep presented in Figure 3b, the current densities presented here are considerably smaller, and it is attributed to the non-stationary nature of the galvanodynamic sweep.

Likewise in Figure 5, Figure 7 summarizes the dynamic behavior presented in Figure 6, in terms of the observed states as a function of the applied current density. With the increase of the applied current density, the system transited from stable steady state (SSSI) to type I mixed-mode oscillations (MMO I), and then reached a new stable steady state (SSSII). After that the system went into the second oscillation region with the current density increasing. The oscillation mode changed from simple small oscillations (SO) to bursting oscillations (BO), type II mixed-mode oscillations (MMO II), and the oscillatory amplitude of the potential increases to about 0.500 V. Then the system went to damped oscillation state (DO) before reaching the stable steady state (SSSIII).

Mixed-mode oscillations (MMOs) is the generic term to describe the regular organization of a periodic sequence of oscillations of different amplitudes, and these enticing phenomena occurs in many systems [25-31]. The rich scenario of MMOs observed here under both potential and current control was found to be rather robust and reproducible and thus qualify the thiosulfate/gold system as a candidate for further investigations aiming at specific goals. Further developments in terms of modeling, however, calls for a deeper understanding of the surface chemistry involved; we are currently working in this respect.

3.3 Electrical Characterization

Ohmic drop compensation. In order to characterize the oscillations described above, we firstly investigated the role of the electrode potential. The solution resistance, as measured by

impedance at high frequency, amounts to around 2.20 Ω. We compensate this resistance using the iR compensation circuit in the Autolab PGSTAT 302N workstation, the resulting *j-E* curve of 0.400 mol dm^{-3} $Na_2S_2O_3$ with buffer (pH 6.0) on gold electrode is presented in Figure 8. When no resistance is compensated in this system, oscillations are evidently observed in the positive-going potential sweep, as seen in Figure 3a (or Figure 8a). Three distinct oxidation peaks and two oscillatory regions exist in the positive potential scan process. It is interesting to note that when the resistance is compensated, oscillations are suppressed (Figure 8b). From these experiments we can conclude that the electrode potential is an essential variable [32], in the sense that oscillations can be described only if this variable is considered.

Electrochemical Impedance Spectroscopy. EIS experiments were conducted to further classify the oscillatory regions described above. Figure 9 illustrates the EIS spectra (100 kHz - 0.01 Hz) of 0.400 mol dm^{-3} $Na_2S_2O_3$ with buffer (pH 6.0) on gold electrode obtained at some selected applied potentials (A to D) in different potential regions in Figure 8b. When the potential is held at 0.950V on the negative slop of *j-E* curve in the first oxidation region (Figure 8b), the EIS spectrum shows that the system has a negative resistance in the real axis at low frequencies shown in Figure 9a, resulting from formation of a gold sulfide layer. The formation of gold sulfide layer in this potential region causes the electrode surface blockage and the active sites of the electrode are considerably reduced. Consequently, the increase of potential results in the drop of current density. At E = 1.300 V and 1.425 V, the EIS results of both potentials go through a negative differential resistance and the impedance of zero frequency locates in the fourth quadrant of complex plane, seen in Figure 9b and c. Therefore, the character of the hidden N-shaped negative differential resistance (HN-NDR) was discovered in two regions along the positive slopes of *j-E* curves. In these two regions,

formation of different gold oxides are likely the cause of the NDRs. The adsorption and other physical processes of intermediates and/or products on the electrode may induce the negative feedbacks of HN-NDR oscillations. When the potential was increased to about 1.6 V, the surface becomes passivated, and no NDR was observed.

From the perspective of the phenomenological analysis in the linear sweep voltammetric curve, as well as the potentiostatic and galvanostatic curves, there are two oscillatory regions, which show the system has both current and potential oscillations. With resistance compensation, the oscillation amplitudes in both regions were reduced or even disappeared. Electrochemical impedance spectroscopy further indicates that the two oscillation regions are of the HN-NDR type [32-34].

3.4 Chemical Characterization – Capillary Electrophoresis (CE) Analysis

Aiming at giving further insight into the chemistry underlying the electrochemical oscillations, we performed capillary electrophoresis analysis of the products formed along the electrocatalytic oxidation of 0.400 mol dm^{-3} $Na_2S_2O_3$ on gold electrode at some selected potentials. The experiments were carried out on a gold disk (20 mm in diameter, the same as previous experiments) with buffer of 1.000 mol dm^{-3} NaH_2PO_4-Na_2HPO_4 (pH 6.0) for two hours of electrolysis at each potential. After the electrolysis the solution composition was analyzed with capillary electrophoresis. The distribution of different oxidation products as a function of the applied potential was presented in Figure 10.

According to this analysis, $S_3O_6^{2-}$ was detected above 0.300 V. The equilibrium reaction and electrochemical oxidation can be given by [35-36]:

$$2S_2O_3^{2-} \leftrightharpoons S_3O_6^{2-} + S^{2-} \qquad \text{(R1)}$$

$$2Au + S^{2-} \rightarrow Au_2S + 2e^- \qquad \text{(R2)}.$$

There is a large amount of $S_4O_6^{2-}$ according to the peak area of CE when the potential increases to 0.600 V, which demonstrates that peak A in Figure 3a is probably associated to the oxidation of $S_2O_3^{2-}$ to $S_4O_6^{2-}$. The reaction can be written as,

$$2S_2O_3^{2-} \rightarrow S_4O_6^{2-} + 2e^- \quad \text{(R3)}.$$

The formation of some $S_5O_6^{2-}$, detected for E > 0.600 V, reads,

$$S_4O_6^{2-} + S_2O_3^{2-} \rightarrow S_5O_6^{2-} + SO_3^{2-} \quad \text{(R4)}.$$

When E > 0.600 V, the SO_4^{2-} ion appeared and its concentration increased with potential (R5-R6). However, $S_4O_6^{2-}$ was the dominant product during the electrolysis at different applied potential until 1.500 V in our CE analysis. The mains reactions in this case are:

$$SO_3^{2-} \rightarrow SO_4^{2-} + 2e^- \quad \text{(R5)}$$

$$2S_2O_3^{2-} + 5H_2O \rightarrow 2SO_4^{2-} + 10H^+ + 8e^- \quad \text{(R6)}$$

It is worth noting that $S_4O_6^{2-}$ disappears at E > 1.800 V. Moreover, when the applied potential is increased to 1.800 V and 2.000 V, $S_6O_6^{2-}$ and $S_7O_6^{2-}$ are detected according to R7 and R8, respectively,

$$S_5O_6^{2-} + S_2O_3^{2-} \rightarrow S_6O_6^{2-} + SO_3^{2-} \quad \text{(R7)}$$

$$S_6O_6^{2-} + S_2O_3^{2-} \rightarrow S_7O_6^{2-} + SO_3^{2-} \quad \text{(R8)}$$

In summary, trithionate, along with gold sulfide layer, and tetrathionate, further transfer converted to polythionate ($S_nO_6^{2-}$, n = 5-7), were produced via different electrocatalytic reaction routes, resulting in two possible negative feedbacks of HN-NDR oscillations proposed in the following section 3.5.

3.5 Preliminary Mechanistic Analysis

Oscillatory regions denoted as B and C in Figure 3a are probably result of the interplay between the electro-oxidation of sulfur-containing species and the inhibition by

surface oxidation. Therefore, the two NDR regions could be in principle due to the different states of surface oxidation. As the system has complex oscillations, it means that there are multiple feedback mechanisms for the two NDR regions. A tentative scenario includes,

$Au_{(aq)} \rightarrow Au^{n+} + ne^-$ (R9),

$Au^{n+} + mH_2O \rightarrow Au(OH)_m^{(m-n)-} + mH^+$ (R10), and

$sAu(OH)_m^{(m-n)-} \rightarrow sAuO_{n/2}+(n\times s)/2H_2O+s\times(m-n)OH^-$ (R11).

Coupled with negative feedbacks such as competitive adsorption between sulfide (R1-R2) and $Au(OH)_m^{(m-n)-}$(or $AuO_{n/2}$), steps R10 and R11, and Au-oxide (or OH adsorption of Au) reduction, R12 and R13, the NDR regions of different n values can produce complex oscillations,

$Au(OH)_m^{(m-n)-} + nS_2O_3^{2-} \rightarrow Au + n/2\ S_4O_6^{2-} + mOH^-$ (R12), and

$AuO_{n/2} + n\ S_2O_3^{2-} + nH^+ \rightarrow Au + n/2\ S_4O_6^{2-} + n/2\ H_2O$ (R13).

However, we should say that different NDR regions corresponds to individual surface passivated states, which need detailed investigation in the future.

4. Conclusions

The electrocatalytic oxidation of thiosulfate on gold electrode in buffered solution of pH 6.0 was investigated. The initial aspect to be pointed out is the very rich dynamics, including highly periodic oscillations and series of mixed-mode states, observed under both galvanostatic and potentiostatic regimes. The system displays supercritical Hopf, period-doubling, homoclinic and bursting bifurcations, especially the period-doubling of mixed-mode oscillation when adjusting the relevant parameters, distributed along two unstable regions. EIS, ohmic resistance compensation, linear sweep curves, as well as the potentiostatic and galvanostatic dynamics indicated that the system displayed HN-NDR oscillations. Capillary Electrophoresis analysis detected $S_3O_6^{2-}$ and $S_4O_6^{2-}$, which indicate

that competitive processes between sulfide formation (R1-R2) and gold-oxide (or OH adsorption) and reduction (R12 and R13) of gold-oxide (or OH adsorption) as the two negative feedbacks of HN-NDR oscillations. $S_nO_6^{2-}$(n = 5-7) was obtained from the reaction between $S_{n-1}O_6^{2-}$ and $S_2O_3^{2-}$.

Mixed-mode sequences observed here evidences a much more robust and intricate dynamics than other comparable systems (see for instance refs. [37-38] for comparison). Besides the sophisticated and presently unknown chemistry of the overall process and also that underlying the feedback loops, the resulting complexity can be attributed to the occurrence of two well-defined consecutive HN-NDR regions. The rich dynamics observed here widens the dynamic complexity in complex structures anticipated for HN-NDR electrochemical systems [39]. From the surface chemistry perspective, this is, for the best of our knowledge, the first report on the oscillatory dynamics during an electro-oxidation reaction on a gold surface. The presented results illustrated the complexity associated to processes such as the degradation of sulfur-containing compounds and also oriented synthesis of sulfur oxides.

Acknowledgements This work was supported by Grants 51221462 from the national Natural Science Foundation of China, the Fundamental Research Fund for the Central Universities (No. 2013XK05) and PADA. HV (grant #306151/2010-3) acknowledges Conselho National de Desenvolvimento Científico e Tecnológico (CNPq) for financial support. HV and MFC acknowledge São Paulo Research Foundation (FAPESP) for financial support (grants #2009/07629-6, #2012/24152-1, and #2013/00216-3).

357

358

359 **References**

360 [1] A. F. Holleman, E. Wiberg, Inorganic Chemistry, Academic Press, San Diego, 2001.

361 [2] M. G. Aylmore, D. M. Muir, Thiosulfate leaching of gold - a review, Minerals
362 Engineering 14 (2) (2001) 135–174.

363 [3] A.H. Hall, R. Dart, G. Bogdan, Sodium thiosulfate or hydroxocobalamin for the empiric
364 treatment of cyanide poisoning, Annals of Emergency Medicine 49 (2007) 806–813.

365 [4] M. Orbán, P. De Kepper, I. R. Epstein, An iodine-free chlorite-based oscillator: the
366 chlorite-thiosulfate reaction in a continuous flow stirred tank reactor, The Journal of Physical
367 Chemistry 86 (1982) 431–433.

368 [5] M. Orbán, I. R. Epstein, Systematic design of chemical oscillators. Part 13. Complex
369 periodic and aperiodic oscillation in the chlorite-thiosulfate reaction, The Journal of Physical
370 Chemistry 86 (1982) 3907–3910.

371 [6]Z. Wang, Q. Y. Gao, C.W. Pan, Y. M. Zhao, A. K. Horváth, Bisulfite-driven autocatalysis
372 in the bromate-Thiosulfate reaction in a slightly acidic medium, Inorganic Chemistry 51
373 (2012) 12062-12064.

374 [7] G. Rábai, M. T. Beck, K. Kustin, I. R. Epstein, Sustained and damped pH oscillation in
375 the periodate-thiosulfate reaction in a continuous-flow stirred tank reactor, The Journal of
376 Physical Chemistry 93 (1989) 2853–2858.

377 [8] M. Orbán, I. R. Epstein, Systematic design of chemical oscillators. 39. Chemical
378 oscillators in group VIA: the copper (II)-catalyzed reaction between hydrogen peroxide and
379 thiosulfate ion, Journal of the American Chemical Society 109 (1987) 101–106.

380 [9] G. Rábai, I. R. Epstein, Systematic design of chemical oscillators. 80. pH Oscillations in a
381 semibatch reactor, Journal of the American Chemical Society 114 (1992) 1529–1530.

382 [10] L. Yuan, Q. Gao, Y. M. Zhao, X. D. Tang, I. R. Epstein, Temperature-induced
383 bifurcations in the Cu(II)-Catalyzed and catalyst-free hydrogen peroxide-Thiosulfate
384 oscillating reaction, The Journal of Physical Chemistry A 114 (2010) 7014–7020.
385 [11] Z. H. Du, Q. Y. Gao, J. M. Feng, Y. C. Lu, J. C. Wang, Dynamic instabilities and
386 mechanism of the electrochemical oxidation of thiosulfate, The Journal of Physical Chemistry
387 B 110 (51) (2006) 26098-26104.
388 [12] K. Krischer, H. Varela, Oscillations and other dynamic instabilities, IN: Handbook of
389 Fuel Cells - Fundamentals, Technology and Applications Editors: W. Vielstich, A. Lamm, H.
390 A. Gasteiger, John Wiley & Sons, Ltd., Chichester. 2 (2003) 679-701.
391 [13] H. Varela, Spatiotemporal pattern formation during electrochemical oxidation of
392 hydrogen on platinum, Chemistry Open 1 (2012) 165-168.
393 [14] H. Angerstein-Kozlowska, B. E. Conway, B. Barnett, J. Mozota, The role of ion
394 adsorption in surface oxide formation and reduction at noble metals: General features of the
395 surface process Original Research Article, Journal of Electroanalytical Chemistry 100 (1979)
396 417-446.
397 [15] L. D. Burke, P. F. Nugent, The electrochemistry of gold: I the redox behaviour of the
398 metal in aqueous media, Gold Bulletin 30 (1997) 43-53 .
399 [16] L. D. Burke, P. F. Nugent, The electrochemistry of gold: II The electrocatalytic
400 behaviour of the metal in aqueous media, Gold Bulletin 31(2) (1998) 39-50.
401 [17] L. D. Burke, O. Connell, AM (2010) The surface electrochemistry of gold. In gold:
402 science and applications, R. Holliday, C. Corti (Eds.), CRC Press (BocaRaton, FL), 2010, 51-
403 67.
404 [18] M. Haruta, Gold as a novel catalyst in the 21st century: Preparation, working mechanism
405 and applications, Gold Bulletin 37(2004) 27-36.

406 [19] F. Plenge, Y. J. Li, K. Krischer, Spatial bifurcations in the generic N-NDR
407 electrochemical oscillator with negative global coupling: Theory and surface plasmon
408 experiments, The Journal of Physical Chemistry B 108(2004) 14255-14264.
409 [20] S. Strbac, R. R. Adzic, Oscillatory phenomena in oxygen and hydrogen peroxide
410 reduction on the Au (100) electrode surface in alkaline solutions, Journal of Electroanalytical
411 Chemistry 337 (1992) 355-364.
412 [21] R. de Lima, H. Varela, Catalytic oxidation of ethanol on gold electrode in alkaline media,
413 Gold Bulletin 41 (2008) 15-22.
414 [22] Y. Kwon, S. C. S. Lai, P. Rodriguez, M. T. AQZZM. Koper, On the catalytic activity of
415 gold towards the oxidation of alcohols in alkaline solution, Journal of the American Chemical
416 Society 133 (2011) 6914–6917.
417 [23] P. Rodriguez, Y. Kwon, M. T. M. Koper, The promoting effect of adsorbed carbon
418 monoxide on the oxidation of alcohols on a gold catalyst, Nature Chemistry 4 (2012) 177-182.
419 [24] C. A. Angelucci, H. Varela, G. Tremiliosi-Filho, J. F. Gomes, The significance of non-
420 covalent interactions on the electro-oxidation of alcohols on Pt and Au in alkaline media,
421 Electrochemistry Communications 33(2013)10-13.
422 [25] R. A. Schmitz, K. R. Graziani, J. L. Hudson, Experimental evidence of chaotic states in
423 Belousov-Zhabotinskii reaction, Journal of Chemical Physics 67(1977) 3040–3044.
424 [26] M. Brøns, K. Bar-Eli, Canard explosion and excitation in a model of the Belousov-
425 Zhabotinsky reaction, The Journal of Physical Chemistry 95(1991) 8706–8713.
426 [27] M. T. M. Koper, Bifurcations of mixed-mode oscillations in a three variable autonomous
427 van der Pol-Duffing model with a cross-shaped phase diagram, Physica D: Nonlinear
428 Phenomena 80(1995)72–94.
429 [28] M. J. B. Hauser, L. F. Olsen, Mixed-mode oscillations and homoclinic chaos in an
430 enzyme reaction, Journal of the Chemical Society, Faraday transactions 92(1996)2857– 2863.

[29] T. J. Kaper, H. G. Rotstein, Introduction to focus issue: Mixed mode oscillations: experiment, computation, and analysis, Chaos 18 (2008) 015101.

[30] N. Baba, K. Krischer, Mixed-mode oscillations and cluster patterns in an electrochemical relaxation oscillator under galvanostatic control, Chaos 18(2008) 015103.

[31] J. G. Freire, J. A. C. Gallas, Stern–Brocot trees in the periodicity of mixed-mode oscillations, Physical Chemistry Chemical Physics 13(2011) 12191–12198.

[32] P. Strasser, M. Eiswirth, M. T. M. Koper, Mechanistic classification of electrochemical oscillators - an operational experimental strategy, Journal of Electroanalytical Chemistry 478 (1999) 50-66.

[33] K. Krischer, In Advances in Electrochemical Science and Engineering; R. C. Alkire, D. M. Kolb, Eds., Wiley-VCH: New York 8(2003) 89-208.

[34] M. Orlik, Self-Organization in Electrochemical Systems II: Spatiotemporal Patterns and Control of Chaos, Springer, Berlin, 2012.

[35] H. Bassett, R. G. Durrant, CXCVII. The inter-relationships of the sulphur acids, Journal of the Chemical society (1927) 1401-1468.

[36] G. Senanay, The Role of Ligands and Oxidants in Thiosulfate Leaching of Gold，Gold Bulletin 38(2005) 170-179.

[37] C. P. Oliveira, N. Lussari, E. Sitta, H. Varela, Oscillatory electro-oxidation of glycerol on platinum, Electrochimica Acta 85 (2012) 674-679.

[38] E. Sitta, M. A. Nascimento, H. Varela, Complex kinetics, high frequency oscillations and temperature compensation in the electro-oxidation of ethylene glycol on platinum, Physical Chemistry Chemical Physics 12 (2010) 15195-1206.

[39] M. A. Nascimento, J. A. C. Gallas, H. Varela, Self-organized distribution of periodicity and chaos in an electrochemical oscillator, Physical Chemistry Chemical Physics 13 (2011) 441-446.

Figure captions

Figure 1. Schematic diagram of the electrochemical apparatus: (1) WE; (2) CE; (3) cycling water; (4) RE; (5) gas tube; (6) reactor; (7) quartz window; (8) CCD camera.

Figure 2. Cyclic voltammogram of 1.000 mol dm^{-3} phosphate buffer (pH 6.0) with gold electrode at a scan rate of 0.01 V s^{-1}. The scan range is between 0 V and 2.000 V.

Figure 3. Potential (a) and current (b) linear sweep curves in 0.400 mol dm^{-3} $Na_2S_2O_3$ with 1.000 mol dm^{-3} phosphate buffer (pH = 6.0). Scan rate is (a) 0.10 mV s^{-1}, and (b) 0.05 mA s^{-1}. The potential and current was scanned from 0 V to 2.000 V(a), and from 0 mA cm^{-2} to 27.00 mA cm^{-2}, respectively.

Figure 4. Current density oscillations of of 0.400 mol dm^{-3} $Na_2S_2O_3$ with buffer (pH 6.0) on gold electrode under potentiostatic control from 0 V to 2.000V. (a) 1.010 V; (b) 1.100 V; (c) 1.155 V; (d) 1.160 V; (e) 1.185 V; (f) 1.230 V; (g) 1.235 V; (h) 1.240 V; (i) 1.320 V; (j) 1.322 V; (k) 1.325 V; (l) 1.328 V; (m) 1.330 V; (n) 1.335 V; (o) 1.345 V; (p) 1.350 V; (q) 1.370 V; (r) 1.375 V; (s) 1.380 V; (t) 1.600 V.

Figure 5. Schematic bifurcation diagram for the electro-oxidation of thiosulfate on gold under potentiostatic control. SSSI-SSIII: stable steady states, SO: simple oscillations, MMO: mixed-mode oscillations, and DO: damped oscillations.

Figure 6. Potential oscillations of 0.400 mol dm^{-3} $Na_2S_2O_3$ with buffer (pH 6.0) on gold electrode under galvanostatic control from 0 to 27.00 mA cm^{-2}. (a) 0.29 mA cm^{-2}; (b) 0.35 mA cm^{-2}; (c) 0.38 mA cm^{-2}; (d) 0.41 mA cm^{-2}; (e) 0.45 mA cm^{-2}; (f) 0.48 mA cm^{-2}; (g) 0.54 mA cm^{-2}; (h) 1.72 mA cm^{-2}; (i) 1.85 mA cm^{-2}; (j) 1.88 mA cm^{-2}; (k) 2.90 mA cm^{-2}; (l) 3.18 mA cm^{-2}; (m) 4.30 mA cm^{-2}; (n) 4.33 mA cm^{-2}; (o) 7.90 mA cm^{-2}.

Figure 7. Schematic bifurcation diagram for the electro-oxidation of thiosulfate on gold under galvanostatic control. SSSI-SSSIII: stable steady states, SO: simple oscillations, MMO: mixed-mode oscillations, DO: damped oscillations and BO: bursting oscillations.

Figure 8. Slow potentiodynamic sweep for the electro-oxidation of 0.400 mol dm^{-3} $Na_2S_2O_3$ with buffer (pH 6.0) on gold electrode at 0.1 mVs^{-1}. (a) without resistance compensation; (b) with 2.20 Ω resistance compensation. (A) 0.950 V, (B) 1.300 V, (C) 1.425V, and (D) 1.600 V.

Figure 9. Electrochemical impedance spectra for the electro-oxidation of 0.400 mol dm^{-3} $Na_2S_2O_3$ with buffer (pH 6.0) on gold electrode at different potentials with compensated resistance 2.20 Ω, (a) 0.700 V, (b) 1.300 V, (c) 1.425 V, and (d) 1.600 V.

Figure 10. Species distribution as the function of the applied potential for the electrochemical oxidation of thiosulfate on gold. Initial concentration of $Na_2S_2O_3$ is 0.40 mol dm^{-3}.

Figure 1

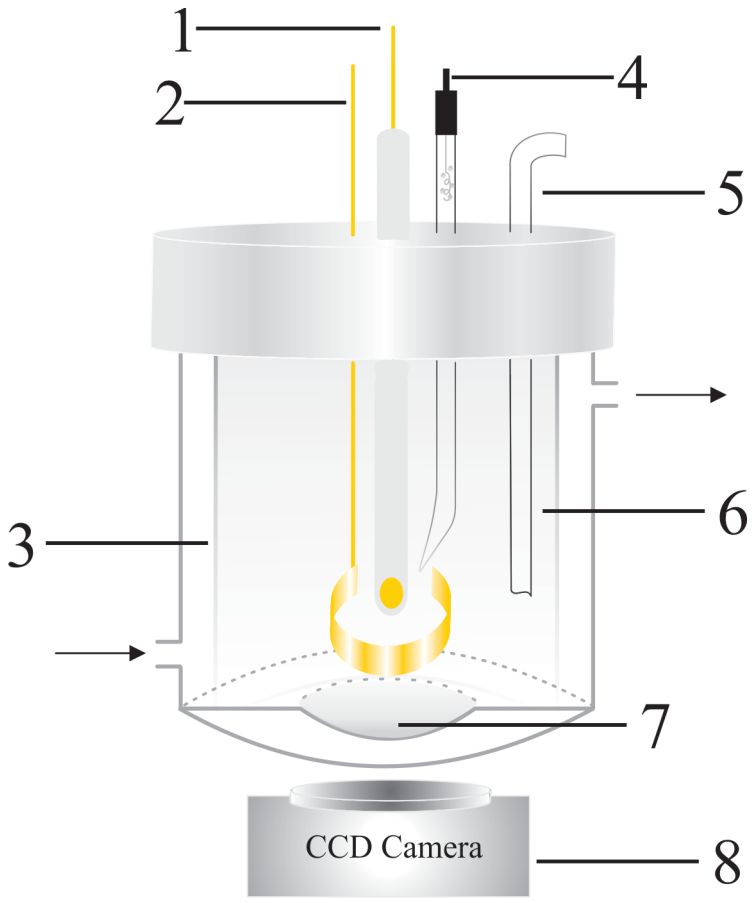

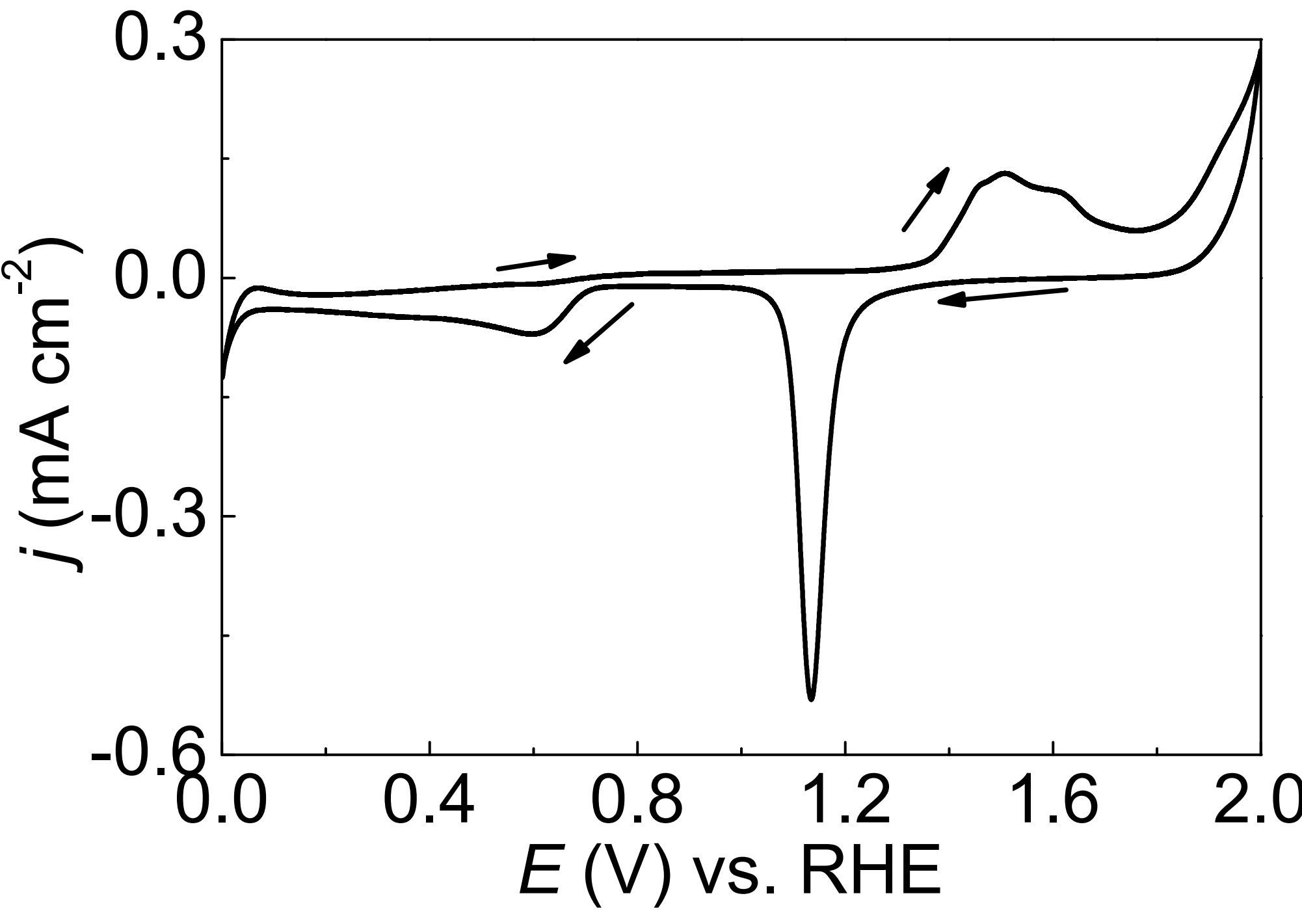
0.3
0.0
-0.3
-0.6
0.0
0.4
0.8
1.2
1.6
2.0
j (mA cm-2)
E (V) vs. RHE

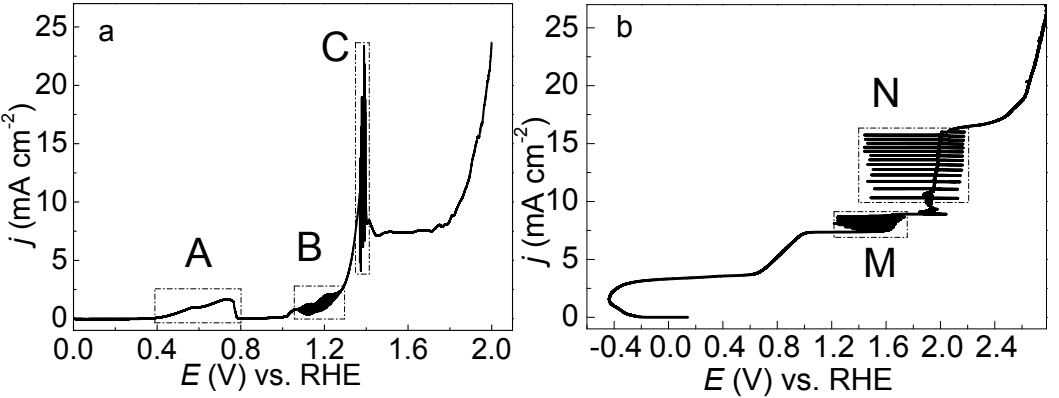
a
b
A
B
C
M
N
j (mA cm-2)
E (V) vs. RHE
0.0
0.4
0.8
1.2
1.6
2.0
-0.4
2.4
0
5
10
15
20
25

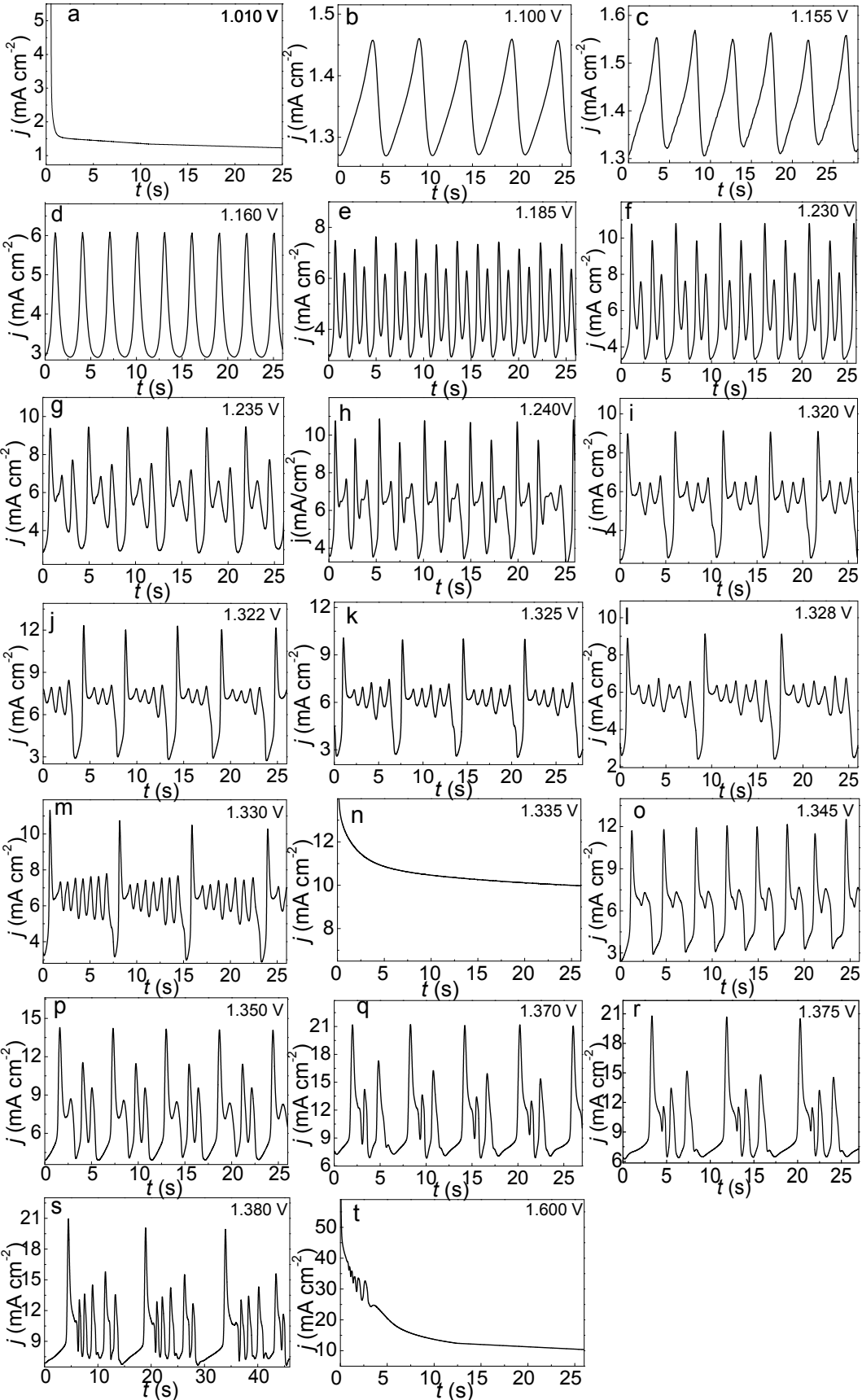
a
1.010 V
b
1.100 V
c
1.155 V
d
1.160 V
e
1.185 V
f
1.230 V
g
1.235 V
h
1.240V
i
1.320 V
j
1.322 V
k
1.325 V
l
1.328 V
m
1.330 V
n
1.335 V
o
1.345 V
p
1.350 V
q
1.370 V
r
1.375 V
s
1.380 V
t
1.600 V
j (mA cm-2)
t (s)


SSS I
SO
MMO I
SSS II
MMO II
DO
SSS III
1.0
1.1
1.2
1.3
1.4
1.5
1.6
E (V) vs. RHE

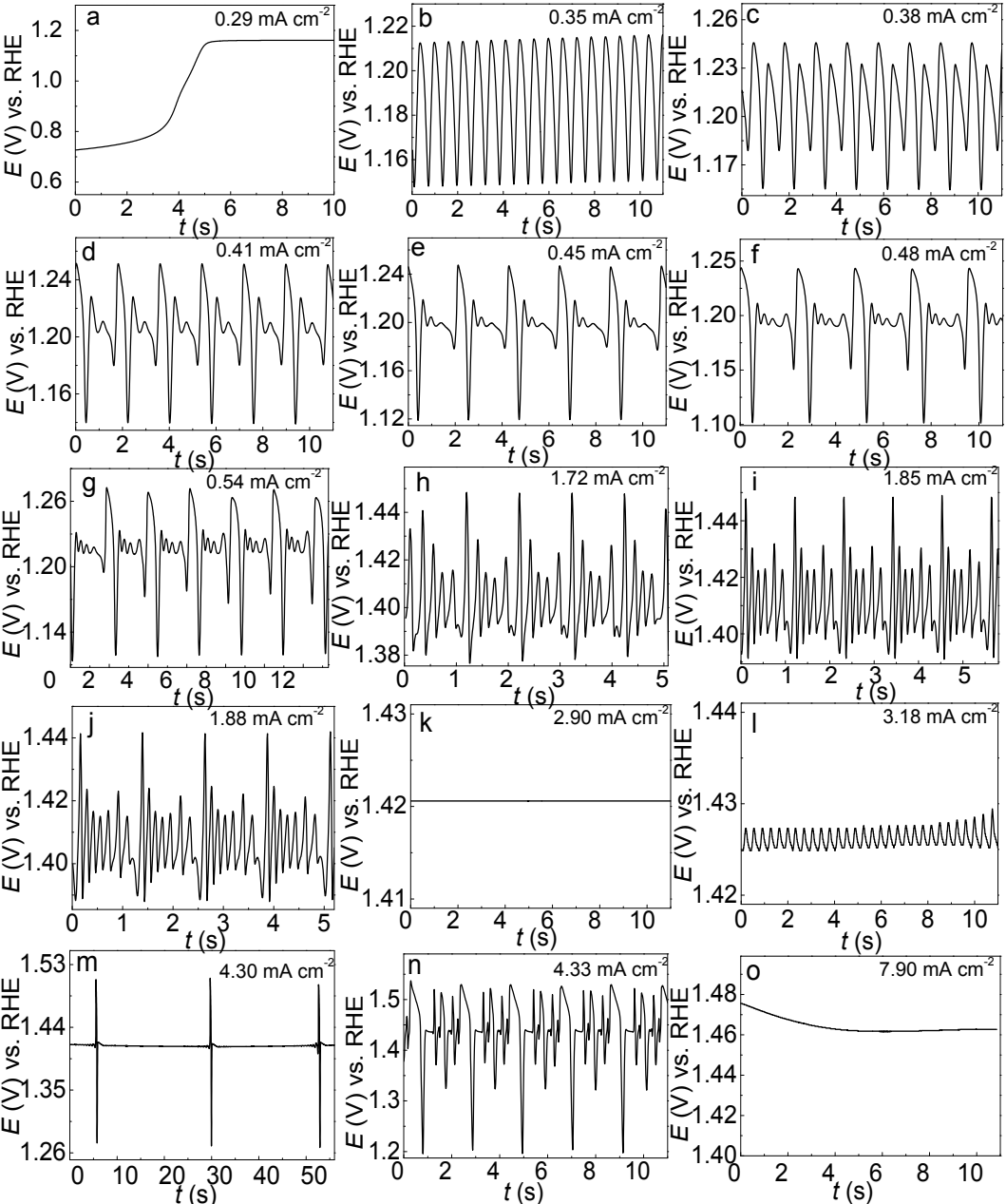
a
0.29 mA cm-2
b
0.35 mA cm-2
c
0.38 mA cm-2
d
0.41 mA cm-2
e
0.45 mA cm-2
f
0.48 mA cm-2
g
0.54 mA cm-2
h
1.72 mA cm-2
i
1.85 mA cm-2
j
1.88 mA cm-2
k
2.90 mA cm-2
l
3.18 mA cm-2
m
4.30 mA cm-2
n
4.33 mA cm-2
o
7.90 mA cm-2
E (V) vs. RHE
t (s)

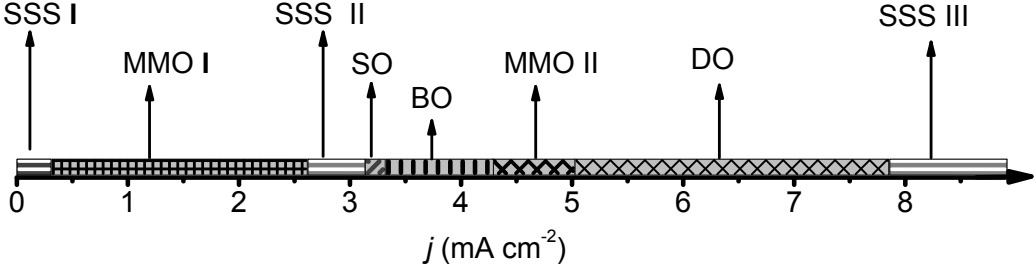
SSS I
MMO I
SSS II
SO
BO
MMO II
DO
SSS III
0
1
2
3
4
5
6
7
8
j (mA cm-2)

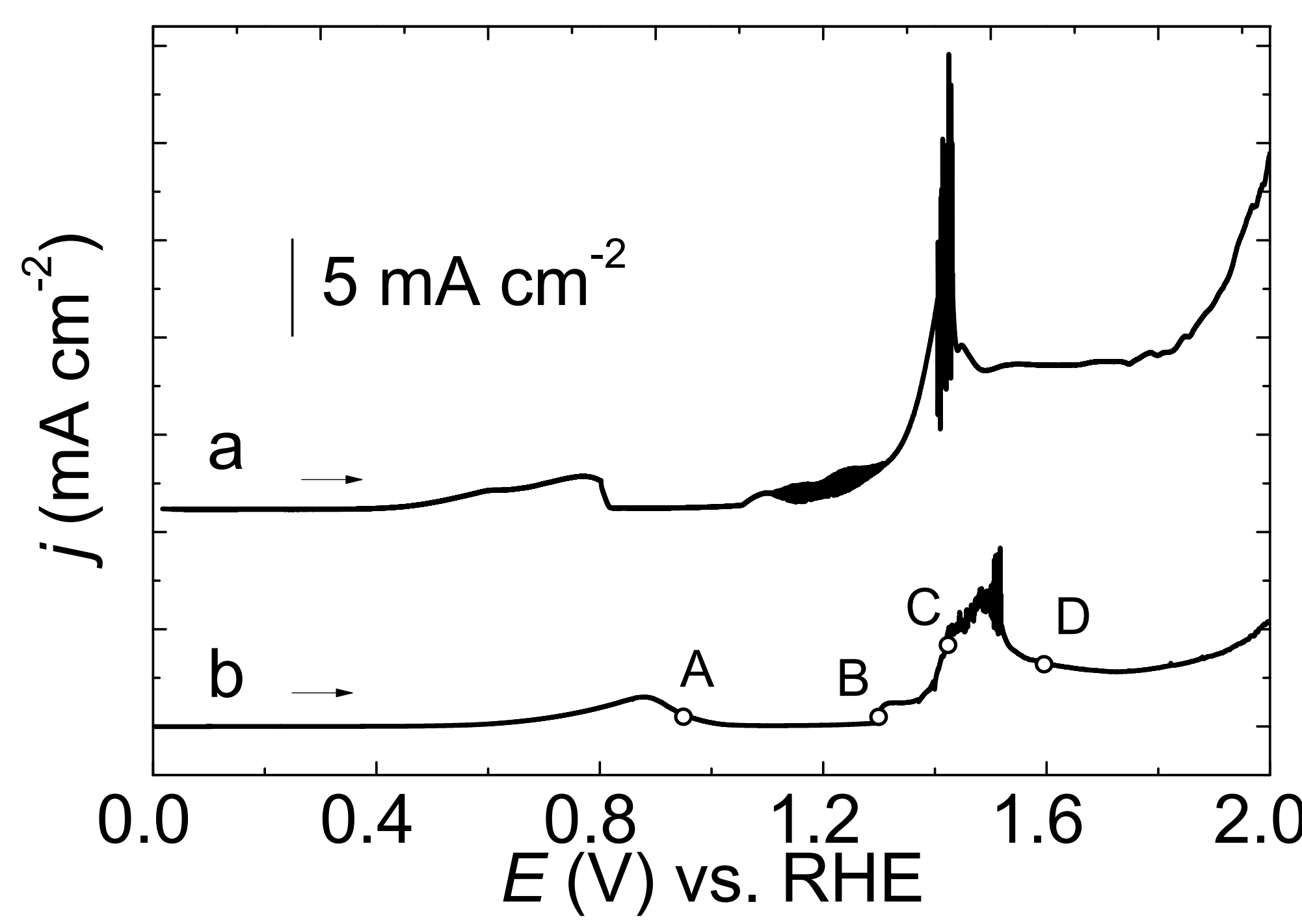
5 mA cm-2
a
b
A
B
C
D
j (mA cm-2)
0.0
0.4
0.8
1.2
1.6
2.0
E (V) vs. RHE

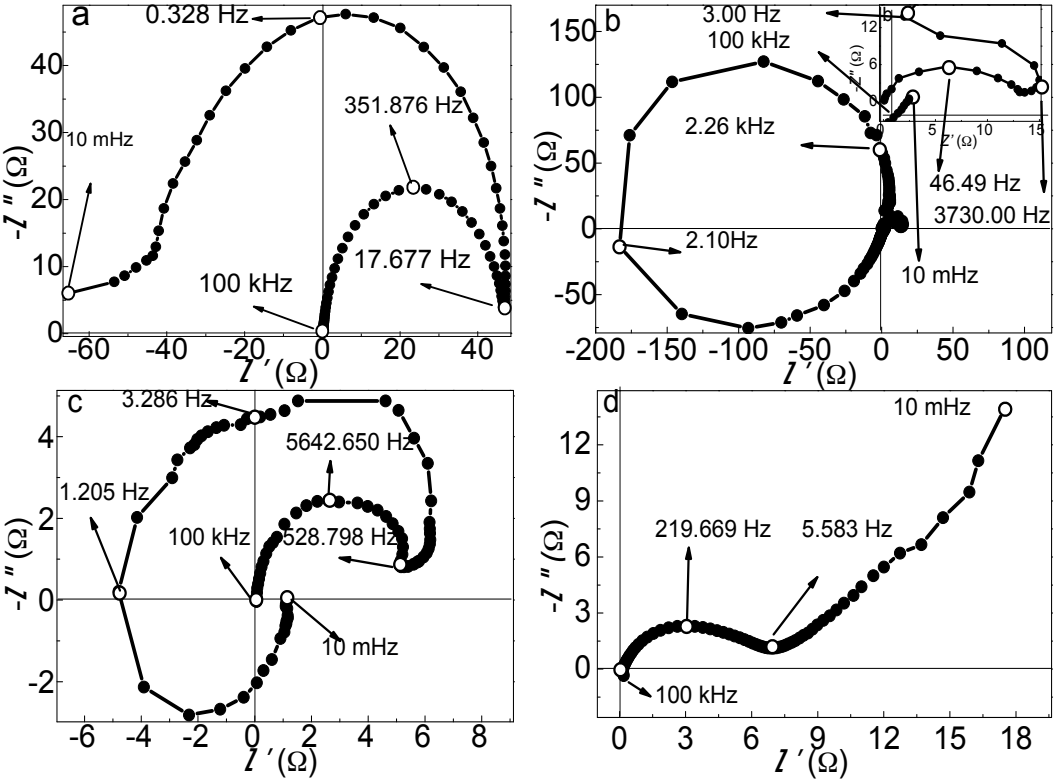
a
0.328 Hz
351.876 Hz
10 mHz
17.677 Hz
100 kHz
-Z ''(Ω)
Z '(Ω)
b
3.00 Hz
100 kHz
2.26 kHz
46.49 Hz
3730.00 Hz
2.10Hz
10 mHz
-Z ''(Ω)
Z '(Ω)
c
3.286 Hz
5642.650 Hz
1.205 Hz
100 kHz
528.798 Hz
10 mHz
-Z ''(Ω)
Z '(Ω)
d
10 mHz
219.669 Hz
5.583 Hz
100 kHz
-Z ''(Ω)
Z '(Ω)

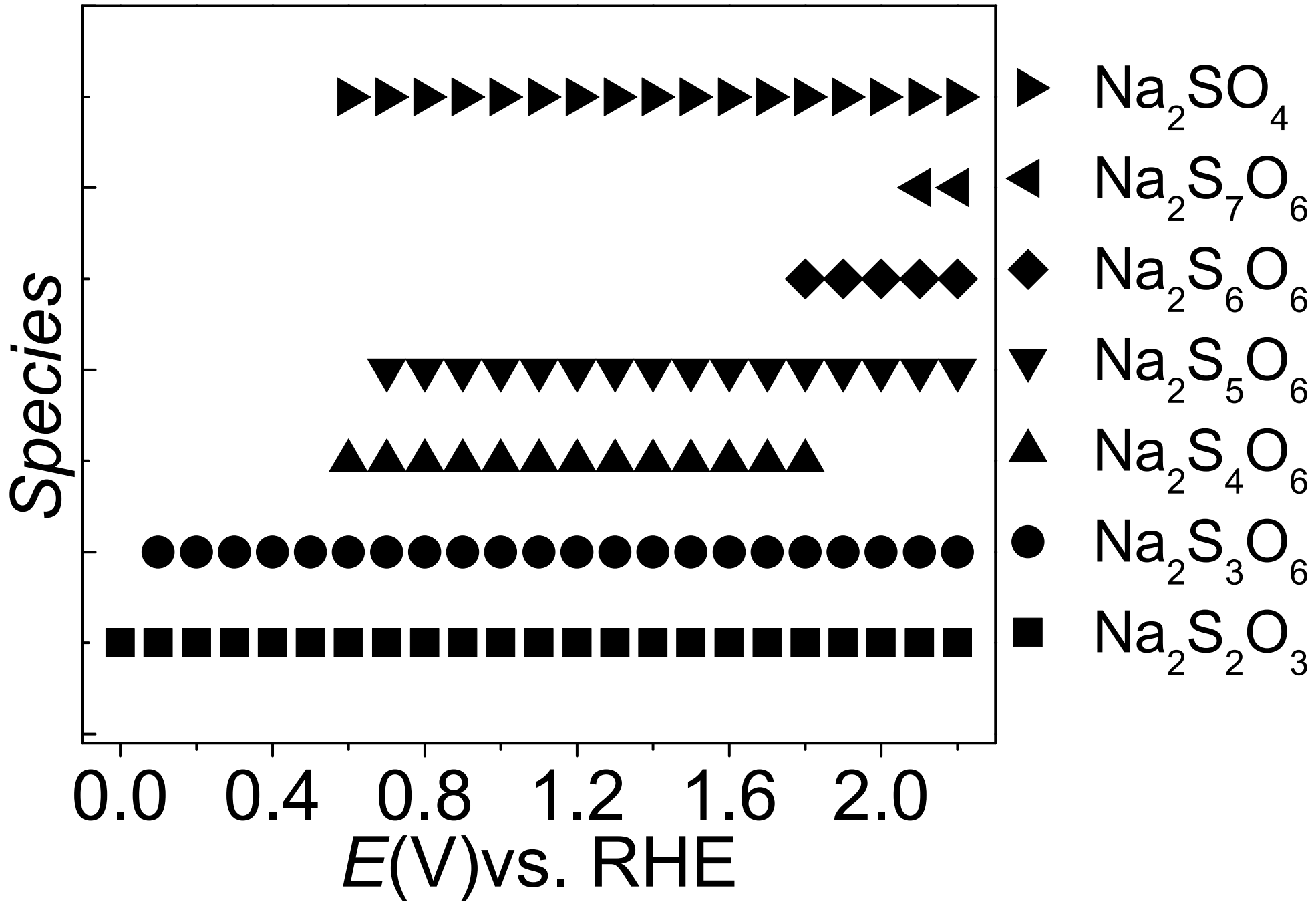
Species
0.0
0.4
0.8
1.2
1.6
2.0
E(V)vs. RHE
Na2SO4
Na2S7O6
Na2S6O6
Na2S5O6
Na2S4O6
Na2S3O6
Na2S2O3

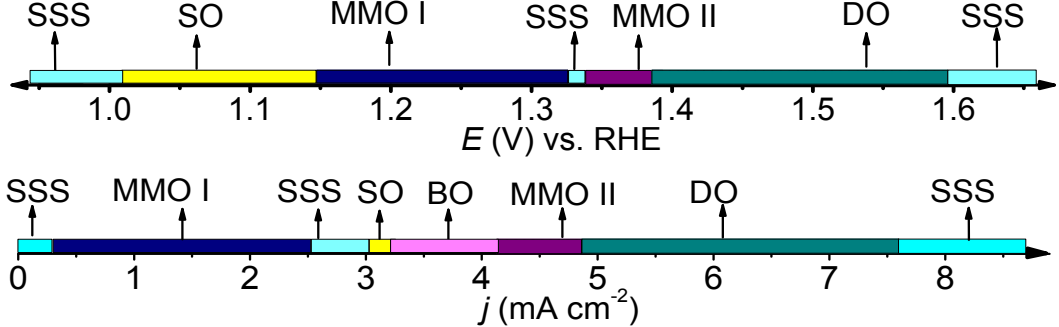

SSS: stable steady state; SO: simple oscillations; MMO: mixed-mode oscillations; DO: damped oscillations; BO: bursting oscillations